Néel skyrmion bubbles in $La_{0.7}Sr_{0.3}Mn_{1-x}Ru_xO_3$ multilayers

Jörg Schöpf,[†,#] Arsha Thampi,[‡,#] Peter Milde,[*,¶,#] Dmytro Ivaneyko,[¶] Svitlana Kondovych,[§] Denys Y. Kononenko,[§] Lukas M. Eng,[¶,@] Lei Jin,[‖] Lin Yang,[†] Lena Wysocki,[†] Paul H. M. van Loosdrecht,[†] Kornel Richter,[⊥] Kostiantyn V. Yershov,[*,§,△] Daniel Wolf,[*,‡] Axel Lubk,[*,‡,▽] and Ionela Lindfors-Vrejoiu[*,†]

†*II. Physics Institute, University of Cologne, 50937 Cologne, Germany*
‡*Institute for Solid State Research, IFW Dresden, Dresden, Germany*
¶*Institute of Applied Physics, TU Dresden, 01062 Dresden, Germany*
§*Institute for Theoretical Solid State Physics, IFW Dresden, 01069 Dresden, Germany*
‖*Ernst Ruska-Centre for Microscopy and Spectroscopy with Electrons, Forschungszentrum Jülich GmbH, 52425 Jülich, Germany*
⊥*Faculty of Sciences, Pavol Jozef Safarik University, Park Angelinum 9, 041 54 Kosice, Slovakia*
#*These authors contributed equally.*
@*ct.qmat, Dresden-Würzburg Cluster of Excellence-EXC 2147, TU Dresden, 01062 Dresden, Germany*
△*Bogolyubov Institute for Theoretical Physics of the National Academy of Sciences of Ukraine, 03143 Kyiv, Ukraine*
▽*Institute of Solid State and Materials Physics, TU Dresden, 01062 Dresden, Germany*

E-mail: peter.milde@tu-dresden.de; k.yershov@ifw-dresden.de; d.wolf@ifw-dresden.de; a.lubk@ifw-dresden.de; vrejoiu@ph2.uni-koeln.de

Abstract

Ferromagnetic $La_{0.7}Sr_{0.3}Mn_{1-x}Ru_xO_3$ epitaxial multilayers with controlled variation of the Ru/Mn content were synthesized to engineer canted magnetic anisotropy and variable exchange interactions, and to explore the possibility of generating Dzyaloshinskii–Moriya interaction. The ultimate aim of the multilayer design is to provide the conditions for the formation of domains with non-trivial magnetic topology in an oxide thin film system. Employing magnetic force microscopy and Lorentz transmission electron microscopy in varying perpendicular magnetic fields, magnetic stripe domains separated by Néel-type domain walls as well as Néel skyrmions smaller than 100 nm in diameter were observed. These findings are consistent with micromagnetic modelling taking into account a sizeable Dzyaloshinskii–Moriya interaction arising from the inversion symmetry breaking and possibly from strain effects in the multilayer system.

Keywords

ferromagnetic perovskite manganites, canted magnetic anisotropy, Dzyaloshinskii–Moriya interaction, magnetic force microscopy, Lorentz transmission electron microscopy

Epitaxial multilayers of ferromagnetic oxides display a wealth of physical properties that are the combined result of the properties of

the bulk ferromagnets subjected to epitaxial growth-related effects, such as strain and reconstructions, of the layer thickness, and of unique interfacial interactions.[1–3] Heterostructures of perovskite manganites (e.g., $La_{0.7}Sr_{0.3}MnO_3$) have been largely investigated, as their ferromagnetic ordering temperature is close to room temperature (RT), the magnetic moment per Mn ion is high and the conduction electrons in its metallic ferromagnetic phase are highly spin polarized.[4,5] Coherent growth on single crystals such as $SrTiO_3$, $(LaAlO_3)_{0.3}$-$(SrAl_{0.5}Ta_{0.5}O_3)_{0.7}$ (LSAT), $NdGaO_3$ or $LaAlO_3$ affects the effective magnetic anisotropy: the tensile strain favors in-plane magnetic easy axes, while compressive strain favors an out-of-plane (OOP) direction of the easy axis.[6] Combining the latter case, also dubbed perpendicular magnetic anisotropy (PMA),[7–9] with (interfacial) Dzyaloshinskii–Moriya interaction (DMI), is the key for realizing topologically non-trivial magnetic textures, such as skyrmions, with small size and high stability even at room temperature (RT), as achieved e.g., in metallic thin films.[10–13]

Notwithstanding, epitaxial ferromagnetic oxide films/heterostructures have been investigated less intensively from the viewpoint of skyrmion formation: e.g., the debate about the formation of tiny magnetic bubbles in ultrathin $SrRuO_3/SrIrO_3$ bilayers and their Néel skyrmion character[14–17] remains unsettled. An attractive prospect of forming skyrmions in ultrathin oxide films is that electric field-effects may be employed for their manipulation.[18] In contrast to $SrRuO_3$ ultrathin films, which have low ferromagnetic transition temperature and strong magetocrystalline anisotropy, for perovskite manganites films the Curie temperature can reach above RT and the magnetocrystalline aniostropy is much weaker.[19] Observations of skyrmions in manganite epitaxial films, such as $La_{0.7}Sr_{0.3}MnO_3$ grown on $NdGaO_3(110)$ substrates[20] or $La_{0.7}Sr_{0.3}Mn_{0.95}Ru_{0.05}O_3$ grown on LSAT(100) substrates,[21] have been recently reported. In the former case, it was proposed that inhomogeneous strain across the relatively thick manganite layers results in a DMI and ultimately in the formation of skyrmions at RT, similar to the inhomogeneous strain-induced formation of magnetic vortex clusters in one-dimensional manganite wires.[22] The particular character of the skyrmions has not been discussed, however. In the case of the Ru-substituted manganite layers grown on LSAT(100), both the Ru substitution and the moderate compressive strain imposed by the substrate are simultaneously affecting the exchange interaction and the effective magnetic anisotropy. Without Ru substitution, 30 nm thick $La_{0.7}Sr_{0.3}Mn_3O_3$ (LSMO) layers epitaxially grown on LSAT show an in-plane magnetic anisotropy and the gradual substitution of Mn by Ru results in increasing PMA: in Ref.[21] it was observed that 5 % Ru substitution (5%Ru-LSMO) was optimal for the formation of skyrmion-like magnetic bubbles. For the layered manganite $La_{1.2}Sr_{1.8}Mn_2O_7$ single crystals, Ru substitution for Mn had also a massive impact on the magnetic anisotropy and on the zero field magnetic domains, resulting in the formation of skyrmion bubbles for higher levels of Ru.[23]

We synthesized $La_{0.7}Sr_{0.3}Mn_{1-x}Ru_xO_3$ epitaxial multilayers building a stack of six manganite layers (each 8 nm thick) of varying Ru/Mn content, with asymmetric top and bottom interfaces (see Fig. 1 and **Supporting Information** Sect. 1 for details). By varying the Ru/Mn content from one layer to the next, the inversion symmetry is broken at all interfaces and a variable strain is introduced in the multilayer system (Ru increases the lattice parameters). Moreover, the strength of the exchange interaction is varied from one layer to the next: The Ru substitution of Mn likely introduces a local antiferromagnetic coupling via superexchange along Ru-O-Mn bonds,[23–25] which may lead to symmetry breaking and spin frustration both inside the layers and at the interfaces.[26] The effective magnetic anisotropy is also different in the individual layers, due to the single ion anisotropy affected by the substitution of magnetic ions (Ru *vs.* Mn)[24] and the modified structure of the Ru-substituted perovskite manganite (varying bond angles and lengths), as well as due to the varying epitaxial strain.

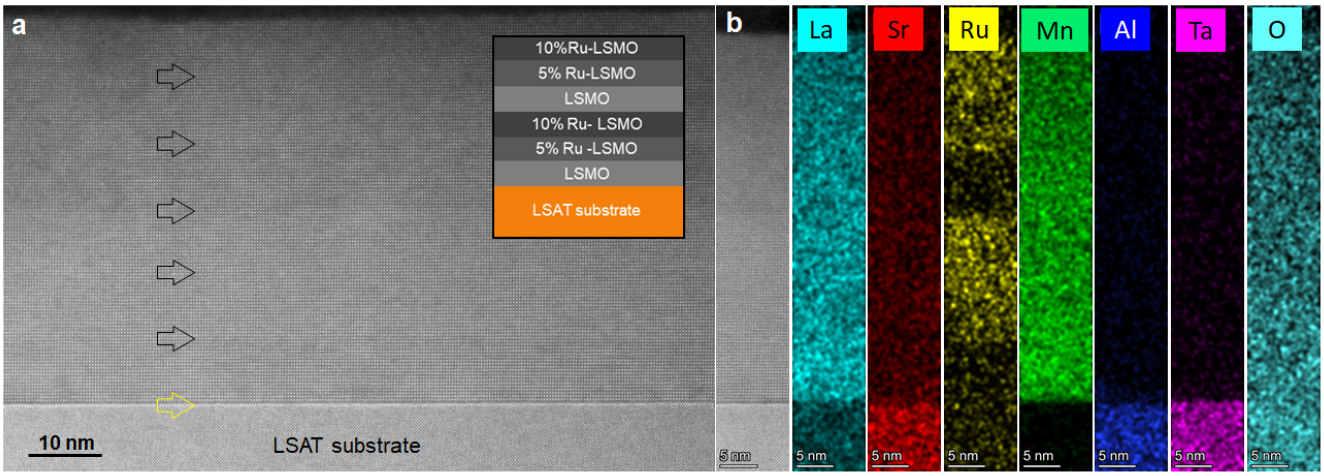

Figure 1: HAADF-STEM microstructure investigations of a cross-section specimen of a 48 nm thick $La_{0.7}Sr_{0.3}Mn_{1-x}Ru_xO_3$ multilayer grown on an LSAT(100) substrate: a) an overview micrograph on which the arrows mark the interfaces with the LSAT substrate and between the six manganite layers with different Ru content (inset: a schematic of the multilayer, indicating the nominal Ru content of the individual layers); b) chemical element distributions across the multilayer, mapped by EDX: the intentional variation of the Ru content (yellow color map) across the stack is clearly observable (scale bar corresponds to 5 nm).

Consequently, inhomogeneous exchange interaction and frustrated magnetic interactions at the interfaces,[26] and an inhomogeneous effective magnetic anisotropy are inherent to these multilayers. Inversion symmetry is broken not only at the interfaces between the layers, but possibly also due to inhomogeneous strain distribution[20] and cation off-centering induced by strain.[27] These jointly contribute to the generation of DMI[28] and thereby to magnetic domains with topologically non-trivial textures in this multilayer system.

The magnetic and magnetotransport properties of the multilayers were investigated at the macro-scale by magnetometry, by magneto-optical Kerr effect (MOKE) measured in polar geometry, and by anomalous Hall effect resistance loops. The temperature and field-dependence of these properties was correlated with the formation of magnetic domains at the micro-scale, observed by magnetic force microscopy (MFM)[8] in as-grown samples, running full hysteresis loops in perpendicular magnetic fields. For in-depth characterization of the magnetic textures, Lorentz transmission electron microscopy (LTEM)[12,21,23,29–33] studies were conducted on backside thinned plan-view TEM lamellas. We consistently observed the formation of magnetic stripe domains[8] as well as their nucleation from and fragmentation into isolated bubbles at low temperatures (below $\approx$ 100 K). The magnetic domain morphology and magnetization behavior observed by MFM changed significantly above 200 K, in accordance with the change of the effective magnetic anisotropy observed by macro-scale magnetometry. In this temperature regime, we observed inconsistencies between the MFM and Lorentz TEM results, which is why we focus on the low temperature regime in this study. The interpretation of the experimental studies was supported by micromagnetic modelling taking into account exchange, DMI, uniaxial anisotropy and dipolar interactions.

The epitaxial character of the multilayers is readily visible in an high-angle annular dark field scanning transmission electron microscopy (HAADF-STEM) overview micrograph, displayed in Fig. 1a: the arrows mark the position of the interfaces between the six $La_{0.7}Sr_{0.3}Mn_{1-x}Ru_xO_3$ layers of different Ru composition (see inset for a schematic of the multilayer structure). Elemental mapping by energy-dispersive X-ray (EDX) spectroscopy

(Fig. 1b) corroborates the uniform chemical composition within each layer and confirms the change of Ru content at the layer interfaces, following the intended variation from 0 to 10 %.

Macroscopic magnetic properties of the multilayers were investigated by SQUID magnetometry. Magnetic moment as a function of temperature, measured after field cooling with the magnetic field oriented either perpendicular to the multilayer surface (cubic [001] direction) or along two cubic in-plane directions, indicates a Curie temperature slightly higher than 300 K and changes of the magnetic anisotropy with temperature (see **Supporting Information** 2, Fig. S 3). Magnetic moment hysteresis loops measured for different direction of the magnetic field show that the magnetization is neither truly perpendicular nor totally in-plane, but canted[34,35] at all temperatures. The effective magnetic anisotropy of the multilayers has a complex temperature dependence, changing from OOP (at low temperatures) to dominantly in-plane anisotropy above 200 K (see **Supporting Information** Sect. 2, Fig. S3d). Longitudinal MOKE imaging at RT displayed in-plane magnetic domains (tens of microns large) and square in-plane Kerr rotation loops, consistent with an in-plane magnetic easy axis (see **Supporting Information** 2, Fig. S 6). The temperature dependence of the effective magnetic anisotropy results from the competition between dipolar interaction, favoring in-plane magnetization, and magnetoelastic anisotropy (induced by epitaxial compressive stress) along with the magnetocrystalline anisotropy of (orthorhombic) Ru-substituted LSMO,[36] favoring OOP magnetization. The OOP tilted easy axis of our multilayers at low temperatures is likely to affect the magnetic domain morphology, in particular the type of bubble domains that form in perpendicular magnetic field.[37]

Hysteresis loops of the Hall effect resistance of a $La_{0.7}Sr_{0.3}Mn_{1-x}Ru_xO_3$ multilayer, measured in perpendicular magnetic field at various temperatures are discussed in the **Supporting Information** 2 (see Fig. S 4). In Fig. 2 we refer to the Hall loop (only the anomalous Hall effect contribution) and to the Kerr rotation loop measured simultaneously at 80 K, and the two loops are in good agreement. In a previous study on 5%Ru-LSMO films grown on LSAT substrates, pronounced humplike features of Hall loops, similar to those of $SrRuO_3/SrIrO_3$ bilayers,[14] were attributed to a THE contribution resulting from the formation of skyrmions.[21] The Hall loops of our multilayers have no obvious hump features at any temperature. We mention that our Hall resistance investigations of a single 5%Ru-LSMO layer (42.5 nm thick) grown on LSAT(100) under the same conditions as the multilayer did not exhibit humps of the Hall loops, at any temperature from 10 K to 200 K, and the magnetic domain imaging by MFM showed no evidence of Néel skyrmion bubbles.[38] THE contributions may not manifest as pronounced humps necessarily, but rather as dip and hump minute modulations of the Hall loops,[11,39] similar to how our Hall loops behave, especially at high temperatures (see Fig. S 4). The Hall loops agree very well with perpendicular magnetization loops measured by SQUID magnetometry (see Fig. S 5). The loops' shape resembles closely what is often measured for ferromagnetic thin films with PMA or canted magnetization, in which magnetic stripe domains form as an effect of demagnetization[11,35] and are the stable remnant state. Thus, from the shape of the Hall loops, the magnetotransport investigations suggest the formation of magnetic stripe domains and possibly skyrmions. We directly observed the latter by means of MFM and LTEM (see **Supporting Information** Sects. 3 and 4 for the details), as it will be presented next.

Both techniques, MFM and LTEM, are well suitable to observe magnetic domains. While MFM is mostly sensitive to the OOP magnetic induction component at the sample surface, LTEM probes the in-plane components of the magnetic induction projected along the viewing direction. We start with the discussion of the LTEM data and compare them to the MFM results subsequently.

We begin with the microscopic domain structure that corresponds to the macroscopic AHE resistance loops obtained at 80 K (see Fig. S 5b), which we correlated with the

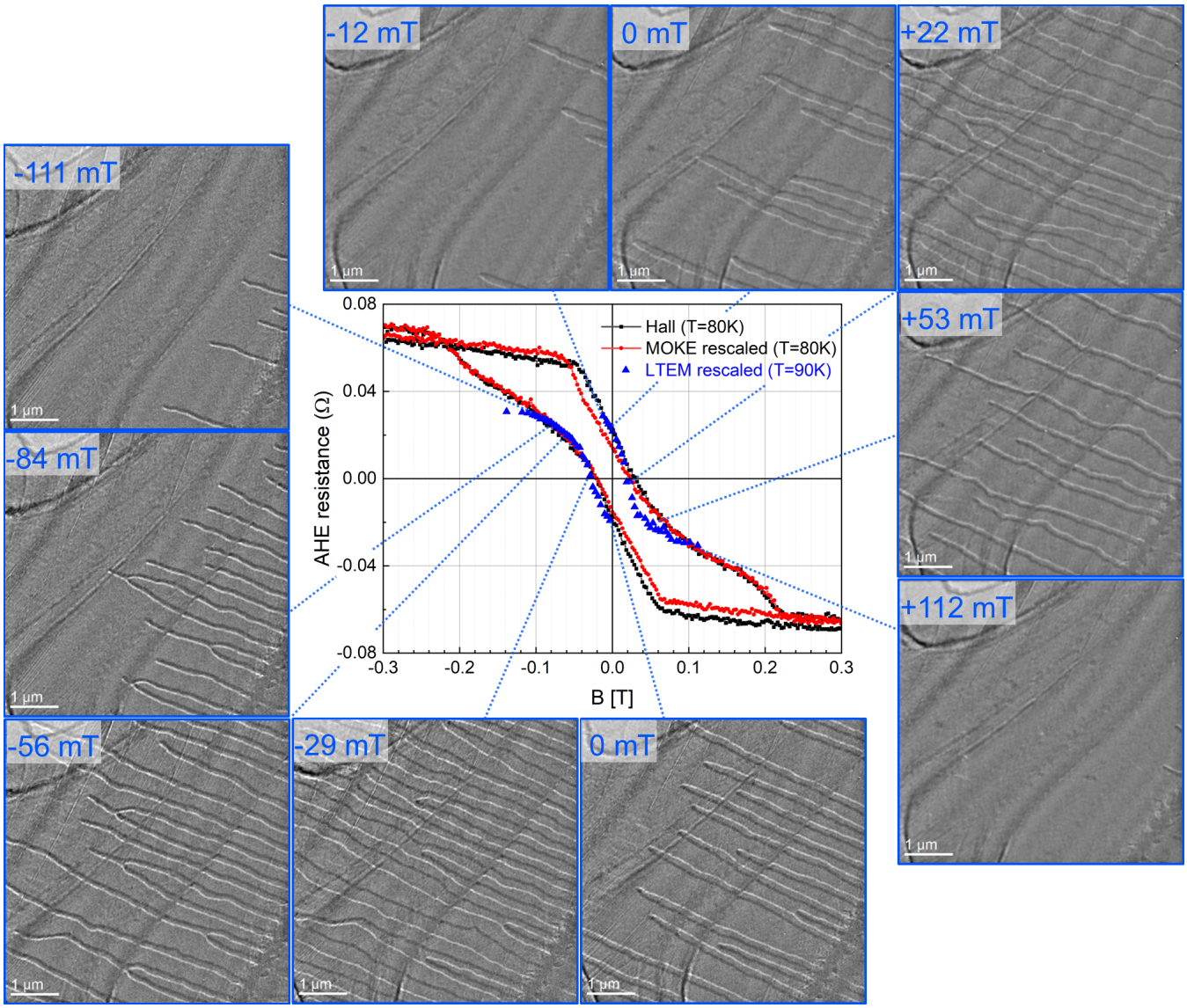

Figure 2: Correlated hysteresis loops of anomalous Hall effect resistance (AHE), Kerr rotation (MOKE), and LTEM measurements as a function of applied magnetic field for the $La_{0.7}Sr_{0.3}Mn_{1-x}Ru_xO_3$ multilayer at a temperature of 80 - 90 K. The magnetic field was always applied perpendicular to the sample surface. Around the hysteresis loops are the LTEM micrographs taken in corresponding magnetic fields, as indicated on the images.

OOP magnetization loops extracted from polar MOKE as well as from LTEM imaging (Fig. 2). The LTEM images shown in Fig. 2 represent snapshots of two field series (shown in Supporting Movie 1 and 2), which are described in the **Supporting Information** 5. Each point of the LTEM magnetization graph (blue triangles) in the central diagram of Fig. 2 was determined by the ratio of the areas within the LTEM images identified as up and down domains, respectively (see **Supporting Information** Sect. 4 for details).

In order to unravel which type of domains, bubbles or skyrmions, is present in the multilayer, we compare the observed LTEM contrasts to theoretical models taking into account the LTEM contrast formation and its sensitivity to the in-plane components of the magnetic induction **B** as depicted in Fig. 3. Whenever the electron beam is aligned parallel to the sample's OOP direction, Bloch DWs separating OOP domains or Bloch skyrmion cores and surroundings provide a strong antisymmetric black-white contrast,[31] whereas Néel DWs or

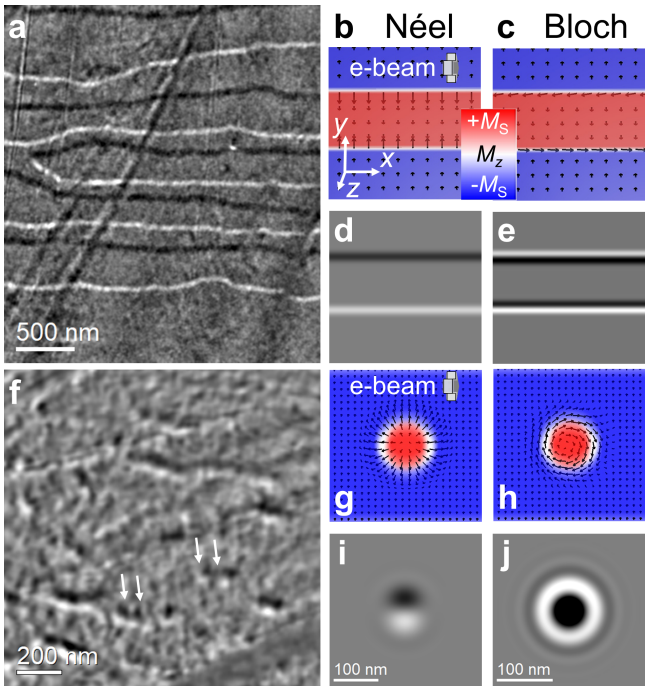

Figure 3: Lorentz TEM (LTEM) imaging of a plane-view prepared $La_{0.7}Sr_{0.3}Mn_{1-x}Ru_xO_3$ multilayer at a temperature of 90 K and comparison with simulation. a) LTEM image capturing stripe domains at an applied OOP field of -19 mT. (b, c) Simulated magnetization of both Néel (b) and Bloch (c) type DWs visualized by the color-coded OOP component M_z in units of saturation magnetization $M_\mathbf{S}$ and arrow plot. (d, e) Simulated LTEM image at -900 µm defocus for Néel (d) and Bloch (e) type DWs assuming the direction of the electron beam 10° tilted with respect to the normal vector of the sample around the $y-$axis as indicated by the gray arrow in (b). f) LTEM image capturing the fragmentation of the stripe domains into Néel skyrmions at an applied OOP field of 300 mT. The white arrows mark the positions of some of the Néel skyrmion bubbles. (g, h) Simulated magnetization of both a Néel (g) and Bloch (h) skyrmion visualized by the color-coded OOP component M_z and arrow plot. (i, j) Simulated LTEM image at -900 µm defocus for Néel (i) and Bloch (j) type assuming the direction of the electron beam 10° tilted with respect to normal vector of sample around the $y-$axis as indicated by the gray arrow in (g).

Néel skyrmions are invisible. To observe the latter, the specimen needs to be tilted around an in-plane axis, such that the OOP component of **B** is partly tilted in-plane.[33] In this case, LTEM images show either black or white DWs depending on the orientation between magnetic field and tilt direction. Consequently, Fig. 3a (see also Fig. SI 8 of Supporting Information Section 4), which was recorded at a sample tilt of about 10° out of the [001] zone axis, reveals Néel-type DWs at a temperature of 90 K. The image was taken a few tens of micrometer away from the sample edge and captured stripe domains at an applied OOP field of -19 mT near the coercive field. Corresponding LTEM image simulations assuming OOP domains with a saturation magnetization 0.5 T,[40,41] separated by either Néel or Bloch type DWs (Figs. 3b,c), a sample thickness of 50 nm and a tilt angle between the specimen's normal and the electron beam of 10° are depicted in Figs. 3d,e, respectively. The comparison with the experiment clearly supports that Néel DWs form in the multilayer. With increasing applied OOP field, the stripe domains become smaller (see Supporting Movies 1,2), ultimately fragmenting into small bubbles at certain positions within the field of view. The LTEM image in Fig. 3f captures the fragmentation of the stripe domains into such bubbles at an applied OOP field of 300 mT. Again, LTEM image simulations of Néel skyrmions (Figs. 3g,i) agree much better with the experimentally obtained contrast (indicated by white arrows in Fig. 3f) than image simulations of Bloch skyrmions / bubbles (Figs. 3h,j). Taking into account that the dominant Néel character could be explained by the presence of a sizeable DMI and stays in contrast to the formation of Bloch bubbles via contribution of PMA, exchange and dipolar interactions (see micromagnetics discussion further below), we refer to these bubbles as Néel skyrmion bubbles in the following. Interestingly, the Néel skyrmion bubbles prefer to nucleate at sample edges (see SI Fig. 9) at high applied fields of ≈350 mT, and not in the middle of the sample, where saturation is reached locally at ≈200 mT. At these field strengths the skyrmion bubbles have a radius of slightly below 50 nm. Note, however, the temperature dependence of the observed stripe domains and skyrmion bubbles

varies from the bulk sample behavior observed with MFM, which is most likely the result of the substrate removal.

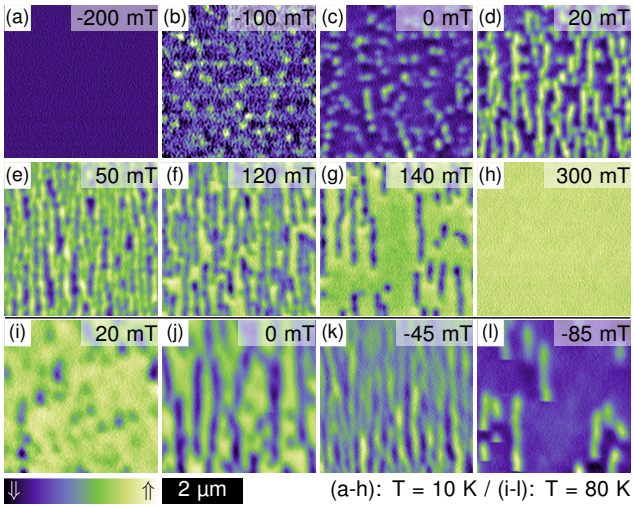

Figure 4: Magnetic force microscopy observation of the evolution of the magnetic pattern with applied OOP field at $T = 10$ K (a-h) and $T = 80$ K (i-l), showing selected images of one hysteresis branch for each temperature. The formation of skyrmion bubbles at the beginning and the end of the magnetization reversal is clearly visible at both temperatures. All images were corrected for both a topographic background and a magnetic background signal. The span of the color bar has been adapted for each image.

In order to study the appearance of magnetic stripe domains and skyrmion bubbles also in as-grown multilayers on intact bulk LSAT substrates, we used MFM at various temperatures and applied magnetic fields. We start with the measurements performed at the lowest temperature $T = 10$ K. After zero field cooling, the applied field was swept in a range of $-2 < B < 2$ T applied perpendicular to the sample surface. Typical images obtained during the up-sweep of the hysteresis measurement are shown in Fig. 4.

Besides a topographic and magnetic background, images for fields $B \leq -200$ mT and $B \geq 180$ mT show no magnetic contrast, see also Fig. 4a,h. The absolute signal strength of these background signals is one order of magnitude smaller than the domain contrast observed during the switching of the OOP magnetization. Details are shown in the **Supporting Information** Sect. 3. For better visualization of the magnetic patterns, all images in Fig. 4 were corrected for both the topographic and the magnetic background signal. The frame size measures 3.8 µm × 3.8 µm for all images, and the span of the color bar has been adapted for each image individually.

When lowering the magnetic field strength, magnetization reversal begins with the nucleation first of skyrmions in the field range between $-200 < B < -100$ mT. They persist in zero field and transform into a stripe pattern for fields slightly larger than zero (see Figs. 4b,c). The highest stripe density is reached for $B \approx 50$ mT, shown in Fig. 4e. As exemplified in Figs. 4f,g, starting at $B \approx 100$ mT piecewise switching of individual stripes transforms the stripe pattern again into the field saturated state. The very same behavior is observed for the down-sweep of the applied magnetic field. A slideshow of the complete data series can be found in the **Supporting Movies 3, 4**.

Next, we compare these results to measurements performed at $T = 80$ K, exemplarily shown in Figs. 4i-l. The general behavior – nucleation of skyrmion bubbles, growth of the latter into stripe domains and piecewise switching of the stripes into the saturated state – equals our findings for $T = 10$ K with slightly changed values for the characteristic magnetic fields, as can be seen in Figs. 4i-l. For, both temperatures and at $B = 0$ T the skyrmion bubble diameter as well as the stripe width measures ≈ 200 nm. Note, however, that the lateral sizes of the skyrmion bubble textures may be substantially smaller than the lateral extension of the corresponding MFM contrast due to the impact of the MFM tip size and the stray field delocalization in the MFM measurement.

Taking that into account the magnetic domain patterns and their field dependency as observed by MFM compare well with our LTEM results at temperatures below 90 K. Thus, we find that the sample properties, in particular the magnetic anisotropy, remained mostly intact after the substrate removal for LTEM investigations. Consequently, the skyrmion bub-

bles observed by MFM can also be identified as Néel type skyrmion bubbles.

The experimentally observed Néel domain walls and skyrmion bubbles in the multilayer system and hence the departure from the typical Bloch bubble physics in PMA thin films suggest the presence of a sizeable DMI (of Néel compatible symmetry, such as interfacial DMI) as underlying driving force. In order to test this hypothesis and to rationalize the experimental findings, we carried out two micromagnetic modelling approaches - an analytical stripe domain model and a full-scale micromagnetic simulation of stripe domains and skyrmion bubbles. In order to employ the stripe domain model,[42] which links the domain width of a periodic stripe pattern to the competition between magnetostatic interaction, uniaxial anisotropy, exchange stiffness, and DMI, we replace the stacked multilayer by a homogeneous film (film thickness 48 nm) described by an effective saturation magnetization, exchange stiffness, DMI strength, and anisotropy. Using that approximation, the stripe domain patterns observed by LTEM measurements at 90 K (Fig. 2) allow for a (rough) estimation of the effective DMI strength in the multilayer film of $D \approx 0.23$ mJ/m^2 (see **Supporting Information** 6). Using the derived material parameters, we carried out full-scale micromagnetic simulations (see **Supporting Information 6** for details) yielding stripe domain structures resembling the experimental patterns and confirming the prediction of the analytical stripe domain model used above. The micromagnetic simulations revealed a continuous transition from Bloch domain walls to Néel domain walls upon increasing DMI strength from zero to a critical DMI strength of $D_{\mathrm{thr}} = 0.23$ mJ/m^2 (see **Supporting Information 6**). This critical DMI strength is roughly similar to the DMI strength estimate obtained from the analytical model, which supports the dominant Néel character of the domain walls observed experimentally. We finally stabilized skyrmion bubbles by increasing the external magnetic field in the micromagnetic model and estimate the radius of the simulated skyrmion bubbles taking into account previously estimated magnetic parameters. The calculations confirm that Bloch-type magnetic bubbles may be stabilized in the absence of DMI by stray fields.[43] Increasing DMI, however, shifts their radius to smaller values and alters the magnetization profile, confirming the stabilization of Néel skyrmion bubbles with $\lesssim 100$ nm radius, as observed experimentally. We stress, however, that the critical magnetic field of ≈ 77 mT for the skyrmion bubble annihilation is lower than observed experimentally, particularly for the thinned TEM samples, which we attribute to the rather larger uncertainties in the employed sample parameters (e.g., magnetic properties, thickness) and the shortcomings of our micromagnetic model (e.g., simplification of the heterostructure). We thus conclude that the presence of an effective DMI may explain the formation of Néel domain walls and skyrmion bubbles in the $La_{0.7}Sr_{0.3}Mn_{1-x}Ru_xO_3$ multilayer.

In summary, we synthesized high quality epitaxial stacks of ferromagnetic $La_{0.7}Sr_{0.3}Mn_{1-x}Ru_xO_3$ layers with varying Ru content in the consecutive layers. The multilayer shows tunable magnetic anisotropy, with dominant out-of-plane magnetic anisotropy below 100 K. High-resolution magnetic imaging techniques revealed the presence of magnetic stripe domains and skyrmion bubbles of Néel character in the same temperature range, in an OOP external magnetic field. Micromagnetic modelling showed that the presence of a sizeable DMI strength $D \approx 0.23$ mJ/m^2 consistently explains the observed domain widths, skyrmion sizes below 100 nm and their dominant Néel character. It remains an open question whether the DMI is of purely interfacial origin or whether an inversion symmetry breaking occurs at the unit cell level, e.g., due to strain induced cation off-centering. We demonstrate the deliberate creation of Néel domains and skyrmion bubbles in epitaxial ferromagnetic oxide thin films with high Curie temperature. This opens the path towards magnetic domains with nontrivial topology at RT: by adjusting the stack design (layer composition, layer thickness, number of layers, etc.), the magnetic interactions and anisotropy may be tuned to expand the temperature range of skyrmion formation. One

can exploit the structural compatibility of manganites with room temperature ferroelectric perovskites, such as $PbTiO_3$, to design hybrid heterostructures with combined functionalities and for electric-field manipulation of skyrmions.

Acknowledgement I. L. -V. and J. S. thank German Research Foundation (DFG) for financing the project A01 within the CRC1238 (Project No. 277146847). I. L.-V. thanks Daniel Jansen and Alexander Bäder for help with the fabrication and AFM of the samples, and Brajagopal Das and Lior Kornblum for XRD measurements. P.M., D.I. and L.M.E. thank the German Research Foundation (DFG) for funding Grants No. EN 434/38-1 and EN 434/40-1 as part of the Priority Program SPP 2137 "Skyrmionics", via the project C05 of the Collaborative Research Center SFB 1143 (project-id 247310070) at the TU Dresden and the Würzburg-Dresden Cluster of Excellence on Complexity and Topology in Quantum Matter – *ct.qmat* (EXC 2147, project-id 390858490). A.L. and D.W. acknowledge financial support by the Collaborative Research Center SFB 1143 (project-id 247310070). S.K. acknowledges the support from the Alexander von Humboldt Foundation. K.Y., S.K., and D.K. thank Ulrike Nitzsche for technical support.

Supporting Information Available

The following files are available free of charge.

- **Supplement.pdf:** Supporting Information on multilayer growth and structural investigations, SQUID magnetometry, Hall effect and MOKE measurements, the applied MFM background correction, LTEM and the transport of intensity reconstruction, as well as details about the stripe domain model, skyrmions and the micromagnetic simulations.
- **Neel-Domains_90K-.mp4:** LTEM magnetic field series applied in out-of-plane direction with respect to the $La_{0.7}Sr_{0.3}Mn_{1-x}Ru_xO_3$ multilayer from +12 mT to -112 mT at 90 K.
- **Neel-Domains_90K+.mp4:** LTEM magnetic field series applied in out-of-plane direction with respect to the $La_{0.7}Sr_{0.3}Mn_{1-x}Ru_xO_3$ multilayer from 0 mT to +138 mT at 90K.
- **MFM_10K_zfc.mp4:** MFM magnetic field series applied in out-of-plane direction with respect to the $La_{0.7}Sr_{0.3}Mn_{1-x}Ru_xO_3$ multilayer after zero field cooling from 0 mT to +2 T to -2 T and finally to +0.5 T at 10 K.
- **MFM_10K.mp4:** MFM magnetic field series applied in out-of-plane direction with respect to the $La_{0.7}Sr_{0.3}Mn_{1-x}Ru_xO_3$ multilayer from 0 mT to +300 mT to -300 mT and back to 0 mT at 10K.

References

(1) Bhattacharya, A.; May, S. J. Magnetic Oxide Heterostructures. *Annual Review of Materials Research* **2014**, *44*, 65–90.

(2) Hellman, F. et al. Interface-induced phenomena in magnetism. *Rev. Mod. Phys.* **2017**, *89*, 025006.

(3) Ijiri, Y. Coupling and interface effects in magnetic oxide superlattices. *Journal of Physics: Condensed Matter* **2002**, *14*, R947–R966.

(4) Haghiri-Gosnet, A.-M.; Renard, J.-P. CMR manganites: physics, thin films and devices. *Journal of Physics D: Applied Physics* **2003**, *36*, R127–R150.

(5) Dörr, K. Ferromagnetic manganites: spin-polarized conduction versus competing interactions. *Journal of Physics D: Applied Physics* **2006**, *39*, R125–R150.

(6) Pesquera, D.; Herranz, G.; Barla, A.; Pellegrin, E.; Bondino, F.; Magnano, E.; Sánchez, F.; Fontcuberta, J. Surface symmetry-breaking and strain effects on

orbital occupancy in transition metal perovskite epitaxial films. *Nature Communications* **2012**, *3*, 1189.

(7) Cape, J. A.; Lehman, G. W. Magnetic Domain Structures in Thin Uniaxial Plates with Perpendicular Easy Axis. *Journal of Applied Physics* **1971**, *42*, 5732–5756.

(8) Hehn, M.; Padovani, S.; Ounadjela, K.; Bucher, J. P. Nanoscale magnetic domain structures in epitaxial cobalt films. *Phys. Rev. B* **1996**, *54*, 3428–3433.

(9) Dieny, B.; Chshiev, M. Perpendicular magnetic anisotropy at transition metal/oxide interfaces and applications. *Rev. Mod. Phys.* **2017**, *89*, 025008.

(10) Moreau-Luchaire, C. et al. Additive interfacial chiral interaction in multilayers for stabilization of small individual skyrmions at room temperature. *Nature Nanotechnology* **2016**, *11*, 444–448.

(11) Raju, M.; Yagil, A.; Soumyanarayanan, A.; Tan, A. K. C.; Almoalem, A.; Ma, F.; Auslaender, O. M.; Panagopoulos, C. The evolution of skyrmions in Ir/Fe/Co/Pt multilayers and their topological Hall signature. *Nature Communications* **2019**, *10*, 696.

(12) Li, M.; Lau, D.; De Graef, M.; Sokalski, V. Lorentz TEM investigation of chiral spin textures and Néel Skyrmions in asymmetric $[Pt/(Co/Ni)_M/Ir]_N$ multi-layer thin films. *Phys. Rev. Materials* **2019**, *3*, 064409.

(13) Chen, X.; Lin, M.; Kong, J. F.; Tan, H. R.; Tan, A. K.; Je, S.-G.; Tan, H. K.; Khoo, K. H.; Im, M.-Y.; Soumyanarayanan, A. Unveiling the Emergent Traits of Chiral Spin Textures in Magnetic Multilayers. *Advanced Science* **2022**, *9*, 2103978.

(14) Matsuno, J.; Ogawa, N.; Yasuda, K.; Kagawa, F.; Koshibae, W.; Nagaosa, N.; Tokura, Y.; Kawasaki, M. Interface-driven topological Hall effect in $SrRuO_3$-$SrIrO_3$ bilayer. *Science Advances* **2016**, *2*, e1600304.

(15) Meng, K.-Y.; Ahmed, A. S.; Baćani, M.; Mandru, A.-O.; Zhao, X.; Bagués, N.; Esser, B. D.; Flores, J.; McComb, D. W.; Hug, H. J.; Yang, F. Observation of Nanoscale Skyrmions in $SrIrO_3/SrRuO_3$ Bilayers. *Nano Letters* **2019**, *19*, 3169–3175.

(16) Malsch, G.; Ivaneyko, D.; Milde, P.; Wysocki, L.; Yang, L.; van Loosdrecht, P. H. M.; Lindfors-Vrejoiu, I.; Eng, L. M. Correlating the Nanoscale Structural, Magnetic, and Magneto-Transport Properties in $SrRuO_3$-Based Perovskite Thin Films: Implications for Oxide Skyrmion Devices. *ACS Appl. Nano Mater.* **2020**, *3*, 1182–1190.

(17) Wysocki, L.; Yang, L.; Gunkel, F.; Dittmann, R.; van Loosdrecht, P. H. M.; Lindfors-Vrejoiu, I. Validity of magnetotransport detection of skyrmions in epitaxial $SrRuO_3$ heterostructures. *Phys. Rev. Materials* **2020**, *4*, 054402.

(18) Ohuchi, Y.; Matsuno, J.; Ogawa, N.; Kozuka, Y.; Uchida, M.; Tokura, Y.; Kawasaki, M. Electric-field control of anomalous and topological Hall effects in oxide bilayer thin films. *Nature Communications* **2018**, *9*, 213.

(19) Ziese, M.; Vrejoiu, I.; Hesse, D. Inverted hysteresis and giant exchange bias in $La_{0.7}Sr_{0.3}MnO_3/SrRuO_3$ superlattices. *Applied Physics Letters* **2010**, *97*, 052504.

(20) Zhang, Y.; Liu, J.; Dong, Y.; Wu, S.; Zhang, J.; Wang, J.; Lu, J.; Rückriegel, A.; Wang, H.; Duine, R.; Yu, H.; Luo, Z.; Shen, K.; Zhang, J. Strain-Driven Dzyaloshinskii-Moriya Interaction for Room-Temperature Magnetic Skyrmions. *Phys. Rev. Lett.* **2021**, *127*, 117204.

(21) Nakamura, M.; Morikawa, D.; Yu, X.; Kagawa, F.; Arima, T.-h.; Tokura, Y.;

Kawasaki, M. Emergence of Topological Hall Effect in Half-Metallic Manganite Thin Films by Tuning Perpendicular Magnetic Anisotropy. *Journal of the Physical Society of Japan* **2018**, *87*, 074704.

(22) Malik, I. A. et al. Inhomogeneous-strain-induced magnetic vortex cluster in one-dimensional manganite wire. *Science Bulletin* **2020**, *65*, 201–207.

(23) Morikawa, D.; Yu, X. Z.; Kaneko, Y.; Tokunaga, Y.; Nagai, T.; Kimoto, K.; Arima, T.; Tokura, Y. Lorentz transmission electron microscopy on nanometric magnetic bubbles and skyrmions in bilayered manganites $La_{1.2}Sr_{1.8}(Mn_{1-y}Ru_y)_2O_7$ with controlled magnetic anisotropy. *Applied Physics Letters* **2015**, *107*, 212401.

(24) Onose, Y.; He, J. P.; Kaneko, Y.; Arima, T.; Tokura, Y. Impact of Ru doping in bilayered manganese oxide $La_{1.2}Sr_{1.8}Mn_2O_7$. *Applied Physics Letters* **2005**, *86*, 242502.

(25) Harano, T. et al. Role of doped Ru in coercivity-enhanced $La_{0.6}Sr_{0.4}MnO_3$ thin film studied by x-ray magnetic circular dichroism. *Applied Physics Letters* **2013**, *102*, 222404.

(26) Hua, E.; Si, L.; Dai, K.; Wang, Q.; Ye, H.; Liu, K.; Zhang, J.; Lu, J.; Chen, K.; Jin, F.; Wang, L.; Wu, W. Ru-Doping-Induced Spin Frustration and Enhancement of the Room-Temperature Anomalous Hall Effect in $La_{2/3}Sr_{1/3}MnO_3$ Films. *Advanced Materials* **2022**, *34*, 2206685.

(27) Sakai, H.; Fujioka, J.; Fukuda, T.; Okuyama, D.; Hashizume, D.; Kagawa, F.; Nakao, H.; Murakami, Y.; Arima, T.; Baron, A. Q. R.; Taguchi, Y.; Tokura, Y. Displacement-Type Ferroelectricity with Off-Center Magnetic Ions in Perovskite $Sr_{1-x}Ba_xMnO_3$. *Phys. Rev. Lett.* **2011**, *107*, 137601.

(28) Xu, Z.; Liu, Q.; Ji, Y.; Li, X.; Li, J.; Wang, J.; Chen, L. Strain-Tunable Interfacial Dzyaloshinskii–Moriya Interaction and Spin-Hall Topological Hall Effect in $Pt/Tm_3Fe_5O_{12}$ Heterostructures. *ACS Appl. Mater. Interfaces* **2022**, *14*, 16791–16799.

(29) Phatak, C.; Petford-Long, A.; De Graef, M. Recent advances in Lorentz microscopy. *Current Opinion in Solid State and Materials Science* **2016**, *20*, 107–114.

(30) Kotani, A.; Nakajima, H.; Harada, K.; Ishii, Y.; Mori, S. Lorentz microscopy and small-angle electron diffraction study of magnetic textures in $La_{1-x}Sr_xMnO_3$ ($0.15 < x < 0.30$):The role of magnetic anisotropy. *Phys. Rev. B* **2016**, *94*, 024407.

(31) Kotani, A.; Nakajima, H.; Ishii, Y.; Harada, K.; Mori, S. Observation of spin textures in $La_{1-x}Sr_xMnO_3$ (x = 0.175). *AIP Advances* **2016**, *6*, 056403.

(32) Kotani, A.; Nakajima, H.; Harada, K.; Ishii, Y.; Mori, S. Field-temperature phase diagram of magnetic bubbles spanning charge/orbital ordered and metallic phases in $La_{1-x}Sr_xMnO_3$ ($x = 0.125$). *Phys. Rev. B* **2017**, *95*, 144403.

(33) Pollard, S. D.; Garlow, J. A.; Yu, J.; Wang, Z.; Zhu, Y.; Yang, H. Observation of stable Néel skyrmions in cobalt/palladium multilayers with Lorentz transmission electron microscopy. *Nature Communications* **2017**, *8*, 14761.

(34) Stickler, D.; Frömter, R.; Stillrich, H.; Menk, C.; Oepen, H. P.; Gutt, C.; Streit-Nierobisch, S.; Stadler, L.-M.; Grübel, G.; Tieg, C.; Yakhou-Harris, F. Domain size in systems with canted magnetization. *Phys. Rev. B* **2011**, *84*, 104412.

(35) Meyer, G.; Bauer, A.; Crecelius, T.; Mauch, I.; Kaindl, G. Magnetization reversal via the formation of stripe domains in ultrathin Fe films on Cu(100). *Phys. Rev. B* **2003**, *68*, 212404.

(36) Konoto, M.; Yamada, H.; Koike, K.; Akoh, H.; Kawasaki, M.; Tokura, Y. Magnetic quasidomain structures in Ru-doped La0.6Sr0.4MnO3 thin films. *Applied Physics Letters* **2008**, *93*, 252503.

(37) Chen, Y.; Lv, B.; Wu, Y.; Hu, Q.; Li, J.; Wang, Y.; Xiong, Y.; Gao, J.; Tang, J.; Tian, M.; Du, H. Effects of tilted magnetocrystalline anisotropy on magnetic domains in Fe_3Sn_2 thin plates. *Phys. Rev. B* **2021**, *103*, 214435.

(38) Wysocki, L. Tunable magnetic anisotropy and magnetotransport properties of epitaxial oxide ferromagnetic heterostructures. PhD Dissertation, University of Cologne, Germany (defence June 2022), 2022.

(39) Tai, L.; Dai, B.; Li, J.; Huang, S. K., Hanshen andChong; Wong, K. L.; Zhang, H.; Zhang, P.; Eckberg, C.; Qiu, G.; He, H.; Wu, D.; Xu, S.; Davydov, A.; Wu, R.; Wang, K. L. Distinguishing the Two-Component Anomalous Hall Effect from the Topological Hall Effect. *ACS Nano* **2022**, *16*, 17336–17346.

(40) Ziese, M.; Vrejoiu, I.; Setzer, A.; Lotnyk, A.; Hesse, D. Coupled magnetic and structural transitions in La0.7Sr0.3MnO3 films on SrTiO3 substrates. *New Journal of Physics* **2008**, *10*, 063024.

(41) Lee, M. S.; Wynn, T. A.; Folven, E.; Chopdekar, R. V.; Scholl, A.; Retterer, S. T.; Grepstad, J. K.; Takamura, Y. Temperature dependence of ferromagnet-antiferromagnet spin alignment and coercivity in epitaxial micromagnet bilayers. *Physical Review Materials* **2017**, *1*, 014402.

(42) Lemesh, I.; Büttner, F.; Beach, G. S. Accurate model of the stripe domain phase of perpendicularly magnetized multilayers. *Physical Review B* **2017**, *95*, 174423.

(43) Büttner, F.; Lemesh, I.; Beach, G. S. Theory of isolated magnetic skyrmions: From fundamentals to room temperature applications. *Scientific reports* **2018**, *8*, 1–12.

TOC Graphic

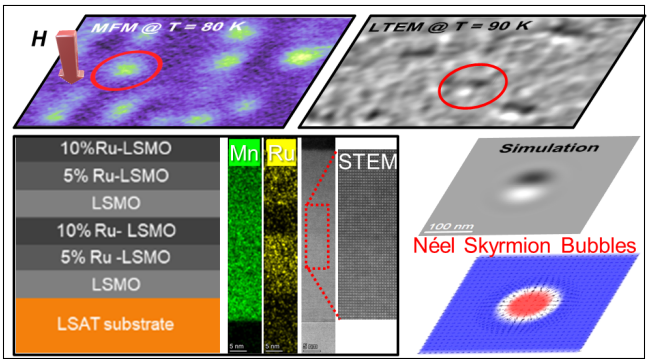
H
MFM @ T = 80 K
LTEM @ T = 90 K
10%Ru-LSMO
5% Ru-LSMO
LSMO
10% Ru- LSMO
5% Ru -LSMO
LSMO
LSAT substrate
Mn
Ru
STEM
Simulation
100 nm
Néel Skyrmion Bubbles